THE ASTROPHYSICAL JOURNAL, 545:701–711, 2000 December 20

ENERGY DIAGNOSES OF NINE INFRARED LUMINOUS GALAXIES BASED ON 3–4 MICRON SPECTRA

MASATOSHI IMANISHI[1]
National Astronomical Observatory, Mitaka, Tokyo 181-8588, Japan
AND
C. C. DUDLEY[2]
Naval Research Laboratory, Remote Sensing Division, Code 7217, Building 2, Room 240B, 4555 Overlook Avenue SW, Washington, DC 20375-5351
Received 2000 June 13; accepted 2000 August 7

ABSTRACT

The energy sources of nine infrared luminous galaxies (IRLGs) are diagnosed based on their ground-based 3–4 μm spectra. Both the equivalent width of the 3.3 μm polycyclic aromatic hydrocarbon (PAH) emission feature and the 3.3 μm PAH to far-infrared luminosity ratio ($L_{3.3}/L_{\rm FIR}$) are analyzed. Assuming that nuclear compact starburst activity in these sources produces the 3.3 μm PAH emission as strongly as that in starburst galaxies with lower far-infrared luminosities, the following results are found. For six IRLGs, both the observed equivalent widths and the $L_{3.3}/L_{\rm FIR}$ ratios are too small to explain the bulk of their far-infrared luminosities by compact starburst activity, indicating that active galactic nucleus (AGN) activity is a dominant energy source. For the other three IRLGs, while the 3.3 μm PAH equivalent widths are within the range of starburst galaxies, the $L_{3.3}/L_{\rm FIR}$ ratios after correction for screen dust extinction are a factor of $\sim$3 smaller. The uncertainty in the dust extinction correction factor and in the scatter of the intrinsic $L_{3.3}/L_{\rm FIR}$ ratios for starburst galaxies does not allow a determination of the ultimate energy sources for these three IRLGs.

Subject headings: galaxies: active — galaxies: individual (IC 694, Arp 220, NGC 6240, Markarian 273, Markarian 231, IRAS 05189−2524, IRAS 08572+3915, IRAS 23060+0505, IRAS 20460+1925, NGC 253) — galaxies: nuclei — galaxies: starburst — infrared: galaxies

1. INTRODUCTION

Infrared luminous galaxies (IRLGs), most of whose huge luminosities are radiated in the far-infrared (40–500 μm) as dust emission ($L_{\rm FIR} \gtrsim 10^{45}$ ergs s^{-1}),[3] are a significant population at the bright end of the galaxy luminosity function (Soifer et al. 1987). Two types of activity, active galactic nucleus (AGN) and starburst, are thought to contribute to the far-infrared emission of IRLGs. The estimate of the relative energetic contributions of these kinds of activity is an important issue for understanding the nature of IRLGs. Furthermore, since the bulk of the cosmic submillimeter background emission can be explained by IRLGs at high redshift (Blain et al. 1999), understanding the energy sources of nearby IRLGs is closely related to the origin of the background emission.

Both AGN and starburst activity produces strong emission lines. Since many emission lines, such as narrow emission lines of hydrogen or H_2 molecules, can be caused by both kinds of activity, it is not easy to distinguish their origin. The polycyclic aromatic hydrocarbon (PAH) emission features can be a powerful tool for separating these kinds of activity and estimating their relative importance because the features are associated only with starburst activity and not with AGN activity (Moorwood 1986). Using the PAH emission feature at 7.7 μm, systematic studies of the energy sources of IRLGs have been reported based on the *Infrared Space Observatory* (*ISO*) spectra at 5.8–11.6 μm (Lutz et al. 1998; Genzel et al. 1998; Rigopoulou et al. 1999). The observed ratios between the 7.7 μm PAH peak flux and 7.7 μm continuum flux of IRLGs were estimated to be as high as those of starburst galaxies with lower far-infrared luminosities, leading these authors to suggest that starburst activity is a dominant energy source for most of the IRLGs they observed. However, the 7.7 μm PAH to far-infrared luminosity ratios of IRLGs are roughly half of those of starburst galaxies (Genzel & Cesarsky 2000). This indicates that observed starburst activity can account for only half of the far-infrared luminosities for IRLGs, although higher dust extinction toward starburst activity in IRLGs could make the intrinsic contribution of starburst activity higher.

In the 5.8–11.6 μm spectra of IRLGs, particularly obscured ones, not only the PAH emission but also broad silicate dust absorption is likely to exist at 8–13 μm (Mathis 1990). Limited wavelength coverage of most *ISO* spectra (5.8–11.6 μm) does not allow the determination of a secure continuum level for many IRLGs, and thus the estimate of the PAH flux could be quantitatively uncertain, as mentioned in Rigopoulou et al. (1999). In fact, the 7.7 μm PAH emission flux of Arp 220, an IRLG for which an *ISO* spectrum with wider wavelength coverage (5–16 μm) is available, could be considerably smaller than that estimated by Rigopoulou et al. (1999), if the continuum level is determined in a different way (Elbaz et al. 1998; Dudley 1999). Furthermore, in the case of another IRLG, IRAS 05189−2524, the reported equivalent widths of the 7.7 μm PAH emission feature based on the *ISO* spectrum differ by a factor of greater than 3 according to different authors (Clavel et al. 2000; Laureijs et al. 2000).

Spectroscopy in the range 3–4 μm can be a powerful method for investigating the energy source of IRLGs, by avoiding the above uncertainty. First, since dust extinction at 3–4 μm is estimated to be as small as that at 7–8 μm ($A_{3.5\ \mu{\rm m}}/A_{7.5\ \mu{\rm m}} \sim 1.2$; Lutz et al. 1996), we can detect signs of obscured energy sources. Next, we can diagnose the rela-

[1] Present address: Institute for Astronomy, University of Hawaii, 2680 Woodlawn Drive, Honolulu, Hawaii 96822.
[2] NRC-NRL Research Associate.
[3] $H_0 = 75$ km s^{-1} Mpc^{-1} and $q_0 = 0.5$ are used throughout this paper.

Report Documentation Page

Form Approved
OMB No. 0704-0188

1. REPORT DATE	2. REPORT TYPE	3. DATES COVERED
2000		**00-00-2000 to 00-00-2000**

4. TITLE AND SUBTITLE	5a. CONTRACT NUMBER
Energy Diagnoses of Nine Infrared Luminous Galaxies Based on 3-4 Micron Spectra	5b. GRANT NUMBER
	5c. PROGRAM ELEMENT NUMBER
6. AUTHOR(S)	5d. PROJECT NUMBER
	5e. TASK NUMBER
	5f. WORK UNIT NUMBER
7. PERFORMING ORGANIZATION NAME(S) AND ADDRESS(ES) **Naval Research Laboratory,Code 7217,4555 Overlook Avenue, SW,Washington,DC,20375**	8. PERFORMING ORGANIZATION REPORT NUMBER
9. SPONSORING/MONITORING AGENCY NAME(S) AND ADDRESS(ES)	10. SPONSOR/MONITOR'S ACRONYM(S)
	11. SPONSOR/MONITOR'S REPORT NUMBER(S)

12. DISTRIBUTION/AVAILABILITY STATEMENT
Approved for public release; distribution unlimited

13. SUPPLEMENTARY NOTES

14. ABSTRACT

15. SUBJECT TERMS

16. SECURITY CLASSIFICATION OF:			17. LIMITATION OF ABSTRACT	18. NUMBER OF PAGES	19a. NAME OF RESPONSIBLE PERSON
a. REPORT **unclassified**	b. ABSTRACT **unclassified**	c. THIS PAGE **unclassified**		**11**	

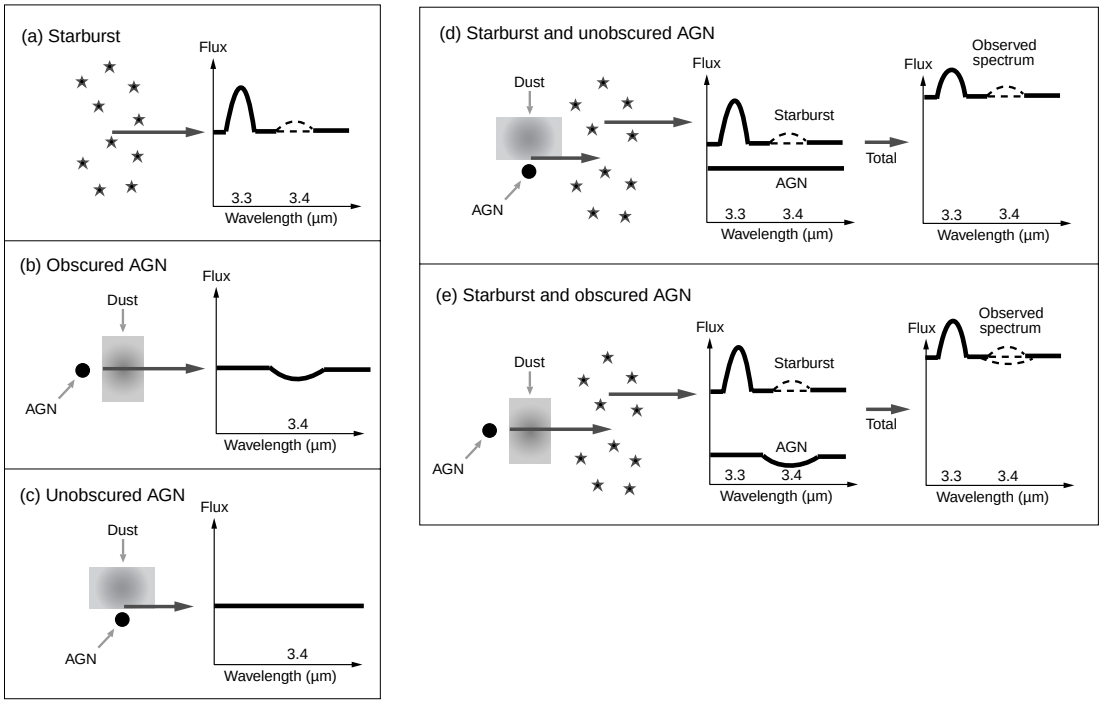

FIG. 1.—Expected 3–4 μm spectral shapes. (*a*) Sources powered by starburst activity. PAH emission is expected to be detected at 3.3 μm and sometimes at 3.4 μm. The effect of dust extinction reduces the PAH and continuum fluxes but does not change the equivalent width of the 3.3 μm PAH emission feature significantly because flux attenuation of the 3.3 μm PAH and 3–4 μm continuum emission is similar. (*b*) Sources powered by obscured AGN activity. The 3.4 μm carbonaceous dust absorption is expected to be detected. (*c*) Sources powered by unobscured AGN activity. The 3–4 μm spectrum should be featureless. (*d*) Sources powered both by starburst and unobscured AGN activity. The 3.3 μm PAH emission feature is expected to be detected, but its equivalent width should be smaller than those of starburst-dominated galaxies because of the contribution of AGN activity to the 3–4 μm continuum emission. (*e*) Sources powered by both starburst and obscured AGN activity. The 3.3 μm PAH emission feature is expected to be detected. When a significant fraction of the 3–4 μm continuum emission originates in the obscured AGN activity, then the equivalent width of the 3.3 μm PAH emission feature is smaller than those of starburst-dominated galaxies, and the 3.4 μm carbonaceous absorption may be detectable if this feature is not veiled by possible PAH emission at 3.4 μm. However, when emission from the obscured AGN activity is so highly attenuated that its contribution to the 3–4 μm continuum emission is very small, the apparent spectral shape is almost the same as those powered only by starburst activity.

TABLE 1

NINE IRLGS AND NGC 253

Object (1)	z (2)	f_{25} (Jy) (3)	f_{60} (Jy) (4)	f_{100} (Jy) (5)	$L_{\rm FIR}$ (ergs s^{-1}) (6)	Spectral Type (7)	Infrared Color (8)
IC 694 (=Arp 299A).....	0.010	21.51[a]	105.82[a]	111.16[a]	44.90[b]	Starburst (1)	...
Arp 220 (=IC 4553)	0.018	8.11	104.08	117.69	45.63	LINER (2)	Cool
NGC 6240	0.024	3.51	23.47	26.55	45.24	LINER (3)	Cool
Mrk 273.....	0.038	2.33	23.70	22.31	45.62	Seyfert 2 (2)	Cool
Mrk 231.....	0.042	8.52	33.60	30.89	45.86	Seyfert 1 (2)	Warm
IRAS 05189−2524.....	0.043	3.52	13.94	11.68	45.49	Seyfert 2 (2)	Warm
IRAS 08572+3915.....	0.058	1.73	7.53	4.59	45.45	LINER (2)	Warm
IRAS 23060+0505.....	0.174	0.46	1.15	0.83	45.63	Seyfert 2 (2)	Warm
IRAS 20460+1925.....	0.181	0.54	0.88	0.48	45.52	Seyfert 2 (4)	Warm
NGC 253.....	3 (Mpc)	117.08	758.69	1044.66	43.76	Starburst[c] (5)	Cool

NOTE.—Col. (1): Object name. Col. (2): Redshift. For NGC 253, a very nearby galaxy, distance in Mpc is shown. Col. (3): *IRAS* 25 μm flux in Jy. Col. (4): *IRAS* 60 μm flux in Jy. Col. (5): *IRAS* 100 μm flux in Jy. Col. (6): Logarithm of far-infrared (40–500 μm) luminosity in ergs s^{-1} calculated with $L_{\rm FIR} = 2.1 \times 10^{39} D({\rm Mpc})^2 (2.58 f_{60} + f_{100})$ ergs s^{-1} (Sanders & Mirabel 1996). Col. (7): Optical spectral type and reference number in parentheses. Col. (8): Far-infrared color: "Warm" ($f_{25}/f_{60} > 0.2$) or "Cool" ($f_{25}/f_{60} < 0.2$).

[a] Total flux of the multinuclei merging system Arp 299. IC 694 is one nucleus of Arp 299. The far-infrared emission of Arp 299 was spatially unresolved with *IRAS*.

[b] The airborne observations of Joy et al. 1989 showed that about 60% of the far-infrared luminosity of Arp 299 comes from the IC 694 nucleus.

[c] Based on a near-infrared spectrum and modeling.

REFERENCES.—(1) Armus, Heckman, & Miley 1989. (2) Veilleux et al. 1999a. (3) Veilleux et al. 1995. (4) Frogel et al. 1989. (5) Engelbracht et al. 1998.

tive importance of AGN and starburst activity using spectral features in the range 3–4 μm. If an IRLG is powered by starburst activity, PAH emission should be detected at 3.3 μm and sometimes at 3.4 μm (Tokunaga et al. 1991). If a source is powered by obscured AGN activity, a 3.4 μm absorption feature of carbonaceous dust grains should be detected (Pendleton et al. 1994), as found in some sources (e.g., NGC 1068; Bridger, Wright, & Geballe 1994; Imanishi et al. 1997). If a source is powered by unobscured AGN activity, a 3–4 μm spectrum should be nearly featureless. Figure 1 summarizes the expected spectral shapes for the above three cases and for the cases of composites of AGN and starburst activity. Finally, since a continuum level both longward and shortward of these features at 3.3–3.4 μm is observable in the L-band (2.8–4.2 μm) atmospheric window of Earth for nearby ($z < 0.18$) sources, there is no serious uncertainty in determining a continuum level.

Ground-based spectroscopy usually makes use of small slit widths, typically less than a few arcseconds. One arcsecond corresponds to greater than a few hundred parsecs in IRLGs at $z > 0.02$. There is currently an increasing amount of evidence based on high spatial resolution imaging studies of infrared 2–25 μm continuum emission that the bulk of the huge dust emission luminosities of IRLGs come from compact (less than a few hundred parsecs) regions powered by AGN and/or compact starburst activity, with little contribution from extended regions (Surace & Sanders 1999; Surace, Sanders, & Evans 2000; Scoville et al. 2000; Soifer et al. 2000). Thus, ground-based 3–4 μm spectroscopy can fully diagnose the properties of dust emission from the energetically important compact regions in most IRLGs. The present study reports ground-based spectroscopy in the wavelength range 3–4 μm of nine IRLGs to investigate their energy sources.

2. TARGET SELECTION

To achieve signal-to-noise ratios higher than 10–20 with a few hours of on-source integration time using the 3.8 m United Kingdom Infrared Telescope (UKIRT), IRLGs brighter than 11 mag at L or L' were selected. The targets are summarized in Table 1. A total of nine IRLGs were observed. Far-infrared luminosities are higher than $\sim 10^{45}$ ergs s^{-1}.

In addition to the IRLGs, NGC 253, a nearby (~ 3 Mpc; Tully 1988) galaxy, was also observed. The emission properties of NGC 253 can be explained by starburst activity only (e.g., Rieke et al. 1980; Engelbracht et al. 1998), and no strong AGN activity has been found. Although its far-infrared luminosity (Table 1) is more than an order of magnitude smaller than those of the IRLGs, this source is powered by compact (~ 100 pc) starburst activity (Kalas & Wynn-Williams 1994). NGC 253 is thus an important nearby source for studying the nature of compact starburst activity found in IRLGs, and its 3–4 μm spectrum can be used as a template of compact starburst activity.

3. OBSERVATION AND DATA ANALYSIS

We used the cooled grating spectrometer (CGS4; Mountain et al. 1990) to obtain 3–4 μm spectra of the IRLGs and NGC 253 with UKIRT on Mauna Kea, Hawaii. An observing log is summarized in Table 2. Sky conditions were photometric throughout the observations. The detector was a 256 × 256 InSb array. The 40 line mm^{-1} grating with 2 pixel wide slit ($=1\farcs2$) was used. The resulting spectral resolution was ~ 750 at 3.5 μm.

Spectra were obtained toward the flux peak at 3–4 μm. A standard telescope nodding technique was employed along the slit to subtract the signal from the sky. The nodding amplitude was $\sim 12''$ except for NGC 253, for which it was $\sim 24''$. The position angles of the slit used are summarized in Table 2. For IRLGs that have clear double nuclei with a small separation (less than several arcseconds; Arp 220, NGC 6240, Mrk 273, and IRAS 08572+3915; Scoville et al. 2000), the position angles were set so that signals from both nuclei were observed simultaneously.

A- to G-type standard stars (Table 2) were observed with almost the same air mass as the target sources to correct for the transmission of Earth's atmosphere. For target sources whose standard stars are A-type, data points at 3.74 and 4.05 μm were removed from final spectra because these data points are affected by, respectively, strong Pfγ and Brα absorption lines in the spectra of A-type stars. The L- or

TABLE 2

OBSERVING LOG

				STANDARD STARS			
OBJECT (1)	DATE (UT) (2)	INTEGRATION TIME (s) (3)	P.A. (deg) (4)	Star Name (5)	L-Band Magnitude (6)	Type (7)	$T_{\rm eff}$ (K) (8)
IC 694	2000 Feb 20–21	2560	0	HR 4761	4.8	F6–8V	6200
Arp 220	2000 Feb 20	3840	90	HR 5634	3.8	F5V	6500
NGC 6240	1999 Sep 9	4800	−19	HR 6629	3.8	A0V	9480
Mrk 273	2000 Feb 20	2560	−35	HR 4761	4.8	F6–8V	6200
Mrk 231	2000 Feb 20	1280	0	HR 4761	4.8	F6–8V	6200
IRAS 05189−2524	1999 Sep 9	3200	−19	HR 1762	4.7	A0V	9480
IRAS 08572+3915	2000 Feb 20	2560	30	HR 3625	4.5	F9V	6000
IRAS 23060+0505	1999 Sep 8	5600	0	HR 8514	4.9	F6V	6400
IRAS 20460+1925	1999 Sep 8	5600	0	HR 7235	3.0	A0V	9480
NGC 253	1999 Sep 9	2400	0	HR 448	4.3	G2IV	5830

NOTE.—Col. (1): Object name. Col. (2): Observing date in UT. Col. (3): Net on-source integration time in seconds. Col. (4): Position angle of the slit; 0° corresponds to the north-south direction. Position angle increases with clockwise on the sky plane. For double nuclei sources with a small separation (Arp 220, NGC 6240, Mrk 273, and IRAS 08572+3915), the position angles were set in such a way that signals from both of the double nuclei enter the slit. Cols. (5)–(8): Standard stars used to correct for the transmission of Earth's atmosphere and to calibrate flux level. Col. (5): Star name. Col. (6): L-band magnitude. Col. (7): Spectral type. Col. (8): Effective temperature.

TABLE 3

L- OR *L'*-BAND MAGNITUDES FROM CGS4 DATA COMPARED WITH MAGNITUDES IN THE LITERATURE

Object	Magnitudes (CGS4)[a]	Magnitudes (Literature)[b]	Reference
IC 694	$L = 10.2$ (1.″2 × 10″)	$L = 10.1$ (4″)	1
Arp 220	$L = 10.7$ (1.″2 × 10″)	$L = 10.5$ (5″)	1
NGC 6240	$L = 10.1$ (1.″2 × 10″)	$L = 9.6$ (9″)	2, 3
Mrk 273	$L = 10.5$ (1.″2 × 10″)	$L = 10.5$ (5″)	1
Mrk 231	$L = 7.2$ (1.″2 × 8″)	$L = 7.4$ (5″)	1
IRAS 05189−2524	$L = 8.6$ (1.″2 × 8″)	$L = 8.4$ (8″)	4
IRAS 08572+3915	$L = 10.1$ (1.″2 × 8″)	$L = 10.0$ (3″)	1
IRAS 23060+0505	$L' = 9.2$ (1.″2 × 8″)	$L' = 9.1$ (6″)	5
IRAS 20460+1925	$L' = 9.5$ (1.″2 × 8″)	$L' = ?$, $L = 9.2$ (12″)	4, 6
NGC 253	$L = 8.4$ (1.″2 × 20″)	$L = 5.7$ (51″)	3

[a] Derived from spectrophotometric CGS4 data taken with a 1.″2 wide slit.

[b] Photometric data from the literature.

REFERENCES.—(1) Zhou, Wynn-Williams, & Sanders 1993. (2) Rudy, Levan, & Rodriguez-Espinosa 1982. (3) Glass & Moorwood 1985. (4) Vader et al. 1993. (5) Hill, Wynn-Williams, & Becklin 1987. (6) Frogel et al. 1989.

L'-band magnitudes of standard stars were estimated from their *V*-band magnitudes, by adopting the $V-L$ or $V-L'$ colors of the stellar types of individual standard stars (Tokunaga 2000).

Standard data analysis procedures were employed using IRAF.[4] First, data of bad pixels were replaced with the interpolated signals of the surrounding pixels. Next, bias was subtracted from the obtained frames, and the frames were divided by a flat image. Then, the spectra of the targets and the standard stars were extracted. Since a secondary nucleus was not clearly recognizable as a distinct nucleus in all cases, spectra were extracted by integrating signals over 8″–20″ along the slit (Table 3). Wavelength calibration was performed using an argon or a krypton lamp and is believed to be accurate within 0.005 μm. The galaxy spectra were divided by those of the standard stars and were multiplied by the spectra of blackbodies with temperatures corresponding to individual standard stars (Table 2). After flux calibration based on the adopted standard star fluxes, the final spectra were produced.

[4] IRAF is distributed by the National Optical Astronomy Observatories, which are operated by the Association of Universities for Research in Astronomy (AURA), Inc., under cooperative agreement with the National Science Foundation.

4. RESULTS

The flux-calibrated spectra are shown in Figure 2. Spectra for some IRLGs were available in the literature, and the new spectra generally agree with previously published spectra. Detailed comparisons of our spectra with previous ones are found in the Appendix.

The comparison of the magnitudes of the CGS4 data with those in the literature is summarized in Table 3. The magnitudes of IRLGs based on the CGS4 data roughly agree with photometric magnitudes measured with larger

TABLE 4

THE PROPERTIES OF THE 3.3 μm PAH EMISSION FEATURE

Object (1)	$\log f_{3.3}$ (ergs s^{-1} cm^{-2}) (2)	$\log L_{3.3}$ (ergs s^{-1}) (3)	$\log L_{3.3}/L_{\rm FIR}$ (4)	Rest $EW_{3.3}$ (nm) (5)
IC 694	−12.23	41.05	−3.85	150
Arp 220	−12.61	41.19	−4.44	82
NGC 6240	−12.40	41.65	−3.59	70
Mrk 273	−12.84	41.61	−4.01	35
Mrk 231	−12.75	41.78	−4.08	2.0
IRAS 05189−2524	−12.96	41.60	−3.89	4.3
IRAS 08572+3915	< −13.87	<40.95	< −4.50	<2.0
IRAS 23060+0505	< −13.88	<41.92	< −3.71	<1.0
IRAS 20460+1925	< −14.30	<41.53	< −3.99	<0.53
NGC 253	−11.56	39.47	−4.29	120

NOTE.—Col. (1): Object name. Col. (2): Logarithm of the observed flux of the 3.3 μm PAH emission feature in ergs s^{-1} cm^{-2}. The flux is estimated by assuming a Gaussian profile whose rest-frame peak wavelength is 3.28–3.30 μm and rest-frame line width in FWHM is 0.04–0.05 μm, as found in the starburst galaxies M82 (Tokunaga et al. 1991) and NGC 253 (this paper). The Gaussian profile can fit the 3.3 μm PAH emission feature reasonably well for all the sources, and systematic errors in the flux estimate using this method are believed to be no more than ∼30%. Col. (3): Logarithm of the observed luminosity of the 3.3 μm PAH emission feature in ergs s^{-1}. Col. (4): Logarithm of the observed 3.3 μm PAH emission to far-infrared luminosity ratio. It is about −3.00 for starburst-dominated galaxies. Col. (5): Rest-frame equivalent width of the 3.3 μm PAH emission feature in nm.

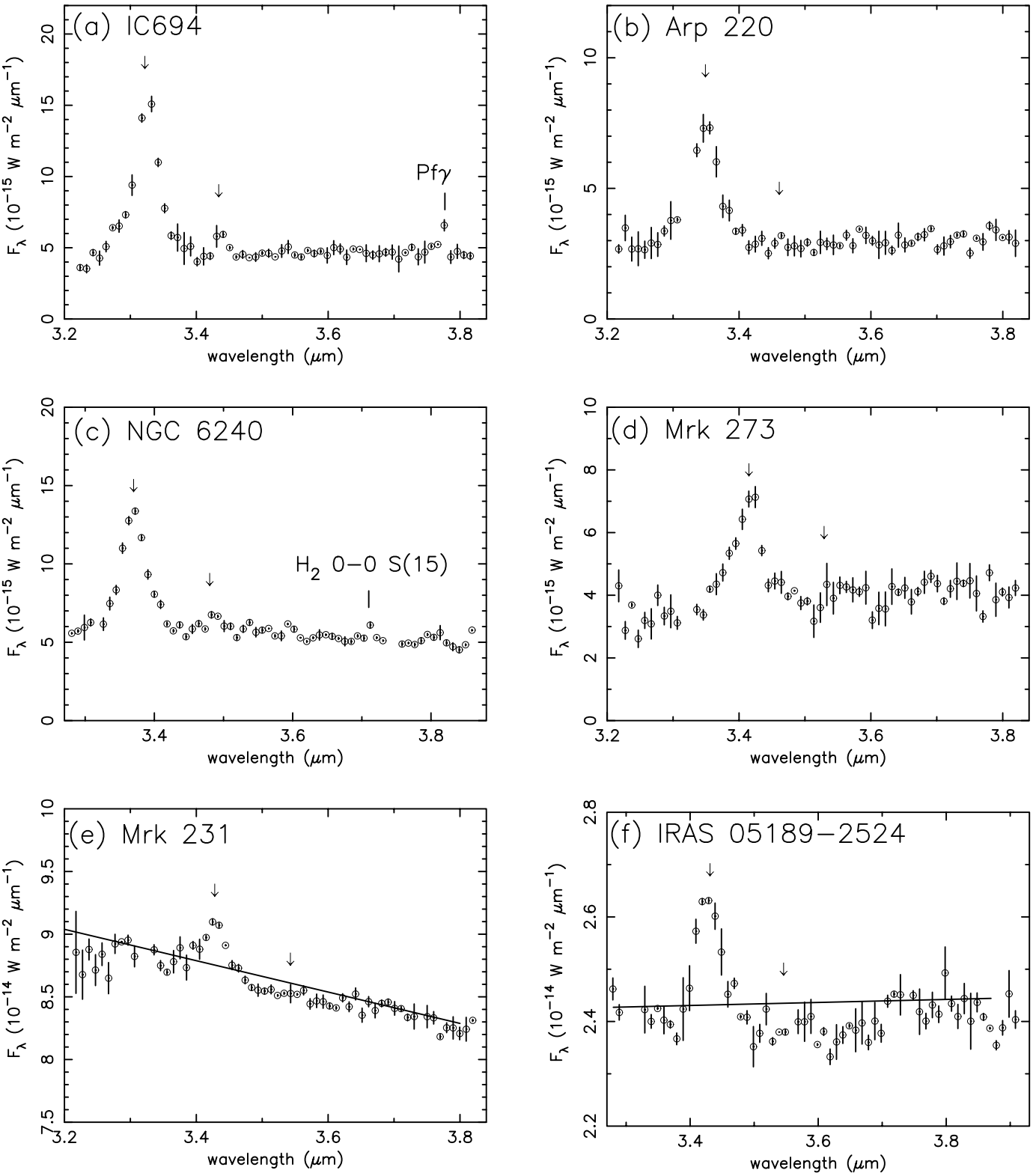

FIG. 2.—Flux-calibrated spectra. The abscissa is the observed wavelength in μm, and the ordinate is the flux in F_λ. The two down-pointing arrows indicate, respectively, the expected wavelengths of the redshifted 3.3 μm PAH emission (rest-frame 3.29 μm) and 3.4 μm absorption (rest-frame 3.4 μm) features. The solid lines in the spectra of Mrk 231, IRAS 05189−2524, IRAS 08572+3915, IRAS 23060+0505, and IRAS 20460+1925 are adopted continuum levels to investigate the 3.4 μm carbonaceous dust absorption feature. Pfγ emission lines are shown in the spectra of IC 694 and NGC 253. In the spectrum of NGC 6240, the H_2 0–0 $S(15)$ emission line is shown. To reduce the scatter of data points in the continuum, spectra are shown with the spectral resolution of $\sim$ 380 except for IRAS 23060+0505 and IRAS 20460+1925, where it is $\sim$200.

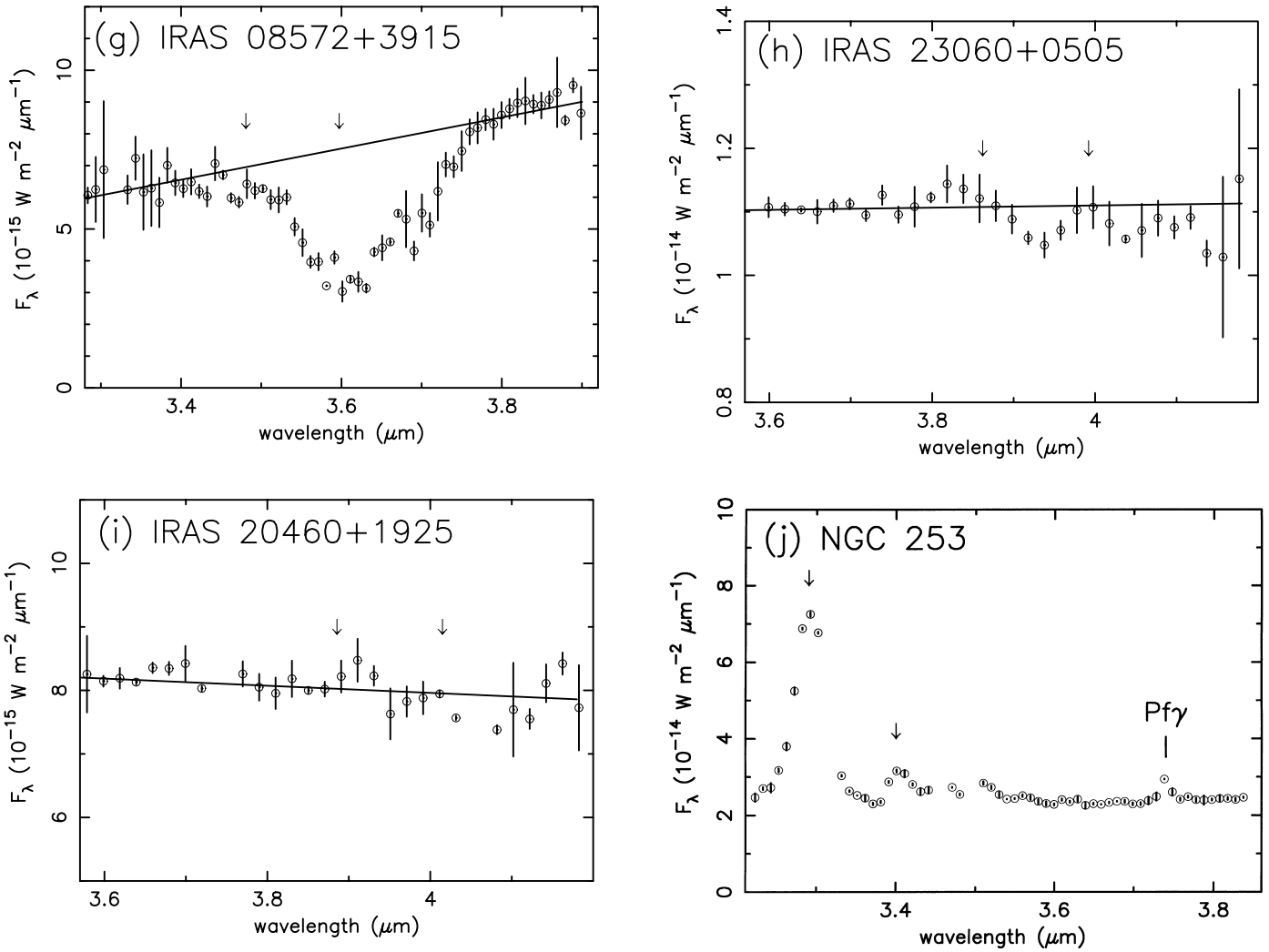

FIG. 2.—*Continued*

apertures, suggesting that nearly all of previously measured 3–4 μm emission is also detected in the CGS4 data.

The spectra of IC 694, Arp 220, NGC 6240, and Mrk 273 are dominated by the 3.3 μm PAH emission and no detectable 3.4 μm carbonaceous dust absorption, as in the case of NGC 253. The spectrum of Mrk 231 shows the 3.3 μm PAH emission and possible 3.4 μm carbonaceous dust absorption, but the reality of the latter feature is currently doubtful. The spectrum of IRAS 05189−2524 shows both 3.3 μm PAH emission and detectable 3.4 μm carbonaceous absorption with an optical depth of $\tau_{3.4} \sim 0.04$. The spectrum of IRAS 08572+3915 is dominated by the 3.4 μm carbonaceous dust absorption feature ($\tau_{3.4} \sim 0.9$). Neither detectable 3.3 μm PAH emission nor the 3.4 μm carbonaceous dust absorption is found in the spectra of IRAS 20460+1925 and IRAS 23060+0505. The fluxes and luminosities of the 3.3 μm PAH emission feature are summarized in Table 4.

In addition to the above features, Pfγ emission lines (rest wavelength of 3.74 μm) are clearly detected in the spectra of IC 694 and NGC 253. The observed fluxes are 2×10^{-14} and 6×10^{-14} ergs s^{-1} cm^{-2} for IC 694 and NGC 253, respectively. In the spectrum of NGC 6240, we attribute the flux excess at 3.71 μm as H_2 0–0 $S(15)$ emission line (rest wavelength of 3.626 μm). Its flux is 1×10^{-14} ergs s^{-1} cm^{-2}. NGC 6240 is known to show strong H_2 emission lines whose strength ratios can be approximated by thermal excitation with the temperature of $\sim$2000 K (Sugai et al. 1997). The comparison with the H_2 1–0 $S(0)$ flux (1.8×10^{-13} ergs s^{-1} cm^{-2}) measured with a $3'' \times 6''$ aperture (Goldader et al. 1995) provides the 0–0 $S(15)$ to 1–0 $S(1)$ flux ratio of 0.06. This ratio is similar to that found in shock gas in the Orion molecular outflow where the H_2-line ratios are roughly fitted by 2000 K thermal emission (Brand et al. 1988).

5. DISCUSSION

In IRLGs, AGN activity and compact starburst activity are likely to coexist spatially close to each other. If energetic ionizing photons from AGN activity penetrate the compact starburst regions and destroy PAHs (Voit 1992) that otherwise should produce the strong 3.3 μm emission feature, the 3.3 μm PAH luminosity could be small in spite of the presence of strong compact starburst activity. However, in IRLGs, the destruction of PAHs in the starburst regions by energetic photons from AGN activity probably does not occur because of the large column density and high pressures in the interstellar medium (Maloney 1999). In the following discussion, it is assumed that compact starburst activity in the IRLGs produces the 3.3 μm PAH emission

intrinsically as strongly as the star formation activity in starburst galaxies with lower far-infrared luminosities, namely, in proportion to the far-infrared luminosities.

5.1. *The Equivalent Width of the 3.3 μm PAH Emission Feature*

For starburst-dominated galaxies, the rest-frame equivalent widths of the 3.3 μm PAH emission feature ($EW_{3.3}$) do not change significantly as a result of dust extinction because flux attenuation of the 3.3 μm PAH emission and 3–4 μm continuum is similar. Thus, very small $EW_{3.3}$ values are most likely caused by the contribution of AGN activity to the 3–4 μm continuum emission.

The rest-frame $EW_{3.3}$ values of the nine IRLGs are summarized in Table 4. The value for NGC 253 is 120 nm, which is nearly a median value for starburst-dominated galaxies (Moorwood 1986). If the scatter of the values is taken into account and IRLGs with $EW_{3.3} = 60$–240 nm are regarded as candidate starburst-dominated galaxies, then only IC 694, Arp 220, and NGC 6240 have $EW_{3.3}$ values as high as those of starburst galaxies and are thus candidate starburst-dominated galaxies. Mrk 273 shows a factor of $\gtrsim 2$ smaller value than those of starburst galaxies, and thus AGN activity is estimated to contribute $\gtrsim 50\%$ of the 3–4 μm continuum flux. The remaining five IRLGs (Mrk 231, IRAS 05189−2524, IRAS 08572+3915, IRAS 23060+0505, and IRAS 20460+1925) have $EW_{3.3}$ ratios more than an order of magnitude smaller, indicating that greater than 90% of the 3–4 μm continuum flux originates in AGN activity. Since the far-infrared to 3–4 μm flux ratio of dust emission heated by AGN activity through a radiative transfer mechanism depends strongly on dust radial density distribution (Ivezic, Nenkova, & Elitzur 1999),[5] conversion from the AGN contribution at 3–4 μm to that at far-infrared wavelengths is not certain. However, the $EW_{3.3}$ values for these six IRLGs (Mrk 273 and the five IRLGs) give no evidence that they are powered predominantly by compact starburst activity.

5.2. *The 3.3 μm PAH Emission to Far-Infrared Luminosity Ratios*

In § 5.1, three IRLGs have $EW_{3.3}$ values as high as those of starburst galaxies. However, large $EW_{3.3}$ values of the IRLGs do not necessarily mean that their far-infrared luminosities are powered predominantly by starburst activity. Although highly obscured AGN activity can contribute to the observed far-infrared luminosity because of negligible extinction in this wavelength range, the contribution of the highly obscured AGN to the 3–4 μm flux can be highly attenuated. As shown in Figure 1*e*, the apparent spectral shapes of galaxies powered both by starburst and highly obscured AGN activity could be nearly the same as those powered only by starburst activity (Fig. 1*a*).

A straightforward means of estimating the energy contribution of compact starburst activity is to estimate the absolute 3.3 μm PAH luminosity and compare it with the far-infrared luminosity. The 3.3 μm PAH emission to far-infrared luminosity ratios ($L_{3.3}/L_{\rm FIR}$) of the IRLGs are summarized in Table 4. The ratios of nearby starburst galaxies with lower far-infrared luminosity are estimated to be $\sim 1 \times 10^{-3}$ (Mouri et al. 1990), although the scatter in this ratio is difficult to estimate because, in the case of nearby starburst galaxies, the ratios are affected by different aperture sizes between 3–4 μm and far-infrared data (Mouri et al. 1990). The observed $L_{3.3}/L_{\rm FIR}$ ratios for all nine IRLGs are less than 3×10^{-4}, a factor of greater than 3 smaller than those of starburst galaxies. The smaller ratios for the six IRLGs with small $EW_{3.3}$ values can be explained naturally by a dominant contribution of AGN activity, while a few mechanisms can explain the smaller ratios in the three IRLGs with large $EW_{3.3}$ values (IC 694, Arp 220, and NGC 6240).

If highly obscured AGN activity contributes significantly to the far-infrared luminosity but little to the 3–4 μm flux as a result of high flux attenuation, then the large $EW_{3.3}$ values and the small $L_{3.3}/L_{\rm FIR}$ ratios can be explained. This is the first possible mechanism.

A second mechanism is the effect of possible signal loss in the CGS4 data. The possible signal loss for NGC 6240 could be as high as 0.5 mag or a factor of 1.6, while that for IC 694 and Arp 220 is a factor of $\lesssim 1.2$. Provided that spectral shape outside the CGS4 slit is the same as that inside it, the possible slit loss could decrease the $L_{3.3}/L_{\rm FIR}$ ratios only slightly.

A third possible mechanism is the effect of dust extinction. The $L_{3.3}/L_{\rm FIR}$ ratios for starburst-dominated IRLGs could be smaller than those of starburst galaxies with lower far-infrared luminosities if dust extinction toward compact starburst activity in the IRLGs is much higher.

For IC 694, Arp 220, and NGC 6240, dust extinction toward starburst regions in the case of a foreground dust screen model could be as high as $A_V \sim 20$ mag (Sugai et al. 1999; Alonso-Herrero et al. 2000), $A_V \sim 45$ mag (Rigopoulou et al. 1999, Fig. 7), and $A_V \sim 7$ mag ($A_K = 0.8$ mag; Sugai et al. 1997), respectively. By adopting a standard extinction curve ($A_L \sim 0.06A_V$–$0.07A_V$; Rieke & Lebofsky 1985; Lutz et al. 1996) and taking possible signal loss into account, the *intrinsic* $L_{3.3}/L_{\rm FIR}$ ratios after correction for dust extinction could be as high as 4–7×10^{-4} for all three. Provided that the $L_{3.3}/L_{\rm FIR}$ ratios of control starburst galaxy samples suffer the effect of dust extinction with $A_V \sim 10$ mag (Rigopoulou et al. 1999, Fig. 7), the intrinsic $L_{3.3}/L_{\rm FIR}$ ratios of starburst-dominated galaxies are estimated to be 1.7–1.9×10^{-3}. The intrinsic $L_{3.3}/L_{\rm FIR}$ ratios for the three IRLGs are a factor of ~ 3 smaller. For reference, the 3.3 μm PAH flux of NGC 253 within our slit is measured to be 2.8×10^{-12} ergs s^{-1} cm^{-2}. The *L*-band magnitude inside our slit is 2.7 mag fainter than the total magnitude of this galaxy (Table 3). If the 3–4 μm spectrum shape outside the slit is the same as that inside it, and if $A_V = 14$ mag is adopted as dust extinction toward starburst regions in this galaxy (Rigopoulou et al. 1999, Fig. 7), then the intrinsic $L_{3.3}/L_{\rm FIR}$ ratio is 1.3–1.5×10^{-3}, consistent with the value of 1.7–1.9×10^{-3} within $\sim 25\%$.

Although dust extinction for Arp 220 was derived based on mid-infrared data, the dust extinction for IC 694 and NGC 6240 was estimated based on near-infrared data. The dust extinction estimate based on near-infrared data could be smaller than that based on mid-infrared data; the latter estimate is thought to be more reliable, particularly in the case of high dust extinction (Genzel et al. 1998). From this viewpoint, it is possible that the intrinsic $L_{3.3}/L_{\rm FIR}$ ratios for IC 694 and NGC 6240 could be higher than our estimate. Further, when dust is mixed with emission sources, the dust extinction correction factors could be higher than that for

[5] Users manual available at http://www.pa.uky.edu/moche/dusty.

a foreground screen dust model (e.g., Genzel et al. 1995). Since the scatter of the intrinsic $L_{3.3}/L_{\rm FIR}$ ratios for starburst galaxies is also poorly known, the energy source of these three IRLGs cannot be determined confidently from our diagnoses.

5.3. *Summary of the Energy Sources Derived from the 3–4 μm Spectra*

The energy sources of the nine IRLGs derived from the 3–4 μm spectra are summarized in Table 5. For IC 694, Arp 220, and NGC 6240, which show strong 3.3 μm PAH emission in equivalent width, it is not clear whether compact starburst activity is the only important energy source or a significant fraction of the luminosity is powered by obscured AGN activity (Figs. 1*a* and 1*e*). Mrk 231 and Mrk 273, which show weak 3.3 μm PAH emission and no detectable 3.4 μm carbonaceous dust absorption, are suggested to be powered by either unobscured or obscured AGN activity (Figs. 1*d* and 1*e*). IRAS 05189−2524, which shows weak 3.3 μm PAH emission and detectable (but weak) 3.4 μm carbonaceous dust absorption, is thought to be powered by moderately obscured AGN activity (Fig. 1*e*). The 3–4 μm spectrum of IRAS 08572+3915 is typical of highly dust-obscured AGNs, and thus this source is most likely powered by highly embedded AGN activity (Fig. 1*b*), as further supported by more detailed study based on 3–20 μm spectroscopy (Dudley & Wynn-Williams 1997; Imanishi & Ueno 2000). The featureless 3–4 μm spectra of IRAS 23060+0505 and IRAS 20460+1925 suggest that these sources are powered by less obscured AGN activity (Fig. 1*c*).

5.4. *Comparison with Other Diagnoses*

5.4.1. *The ISO Spectra*

For Arp 220, NGC 6240, Mrk 273, Mrk 231, IRAS 05189−2524, and IRAS 23060+0505, the 7.7 μm PAH peak flux to 7.7 μm continuum flux ratios were used to diagnose their energy source (Rigopoulou et al. 1999; Laureijs et al. 2000). These ratios and the equivalent widths are a similar (but not identical) concept, and both provide the PAH strength relative to the continuum emission. The conclusions drawn from the 3–4 μm spectra and the *ISO* spectra are compared in Table 5. As mentioned in § 1, a continuum determination based on the *ISO* 5.8–11.6 μm spectra is not easy. When data at 11 μm were used to determine a continuum level (Rigopoulou et al. 1999), the 7.7 μm PAH flux for sources with a strong silicate dust absorption feature could be overestimated. Since a different amount of effect of dust extinction at different wavelengths does not change the relative PAH strengths significantly (§ 5.1), the comparison of the strength of the 3.3 and 7.7 μm PAH emission relative to the continuum can provide useful information on the effect of the silicate dust absorption in the *ISO* spectra.

The relative PAH strengths ($EW_{3.3}$ and 7.7 μm PAH peak to continuum flux ratio) for Mrk 231, IRAS 05189−2524, and IRAS 23060+0505 are much smaller than those of starburst galaxies in both wavelengths. The relative PAH strength for NGC 6240 is the same within 30% as the typical value of starburst-dominated galaxies at both wavelengths. In fact, for NGC 6240, no indication of strong silicate dust absorption was found in ground-based 8–13 μm spectra (Roche et al. 1991; Dudley 1999). However, for Arp 220, the 3–4 μm spectrum provides the $EW_{3.3}$ value of ∼80 nm, slightly smaller than those of starburst-dominated galaxies (∼120 nm), while the *ISO* spectrum provides the 7.7 μm PAH peak to continuum flux ratio of ∼4.2, significantly higher than the average value of starburst galaxies (∼3.0). Also for Mrk 273, the 3–4 μm spectrum gives $EW_{3.3} \sim 35$ nm, a factor of ∼3 smaller than starburst galaxies, while the *ISO* spectrum gives the 7.7 μm PAH peak to continuum flux ratio of ∼1.9, only a factor of ∼1.6 smaller. For Arp 220 and Mrk 273, Dudley (1999) argued that silicate dust absorption plays an important role based on ground-based 8–13 μm spectra. The discrepancy may be caused by the effect of the silicate dust absorption.

The above comparison suggests that, for at least some fraction of IRLGs, the 7.7 μm PAH flux estimated by Rigo-

TABLE 5

SUMMARY OF THE MAIN ENERGY SOURCES FOR THE NINE IRLGS

Object (1)	Spectroscopy (3–4 μm) (2)	*ISO* Spectroscopy (5.8–11.6 μm) (3)	Imaging (8–25 μm) (4)	Spectroscopy (2 μm) (5)
IC 694	SB or SB+AGN	...	...	...
Arp 220	SB or SB+AGN	SB (4.2)	?	...
NGC 6240	SB or SB+AGN	SB (2.6)	...	...
Mrk 273	AGN	SB (1.9)	?	...
Mrk 231	AGN	AGN (0.3)	AGN	AGN
IRAS 05189−2524	AGN	AGN (0.4)	AGN	AGN
IRAS 08572+3915	AGN	...	AGN	...
IRAS 23060+0505	AGN	AGN (<0.1)	...	AGN
IRAS 20460+1925	AGN	...	...	AGN

NOTE.—Col. (1): Object name. Col. (2): Energy source derived by this work. "AGN" and "SB" mean AGN-dominated and starburst-dominated, respectively. "SB+AGN" means both kinds of activity contribute roughly equally. Col. (3): Energy source derived based on the ratio between the 7.7 μm PAH peak flux and 7.7 μm continuum flux. The ratios are shown in parentheses. Adopted from Rigopoulou et al. 1999 except for IRAS 05189−2524, for which the ratio is adopted from Laureijs et al. 2000. The average ratios for starburst galaxies and AGNs are ∼3.0 and ∼0.2, respectively (Rigopoulou et al. 1999). Those with the ratios of greater than 1.0 and less than 1.0 are classified as "AGN" and "SB," respectively (Rigopoulou et al. 1999). Col. (4): Energy source derived from high spatial resolution 8–25 μm imaging (Soifer et al. 2000). Col. (5): Energy source derived from 2 μm spectroscopy (Veilleux et al. 1999b). Those with a detected broad emission line whose luminosity is high enough to account for the far-infrared luminosity by AGN activity are classified as "AGN."

poulou et al. (1999) could be too large because of the use of data affected by silicate dust absorption as a continuum level. In this case, the presence of the silicate dust absorption is underestimated. Highly obscured AGNs show spectra characterized by weak PAH emission and strong silicate dust absorption. Virtually no IRLGs powered by highly obscured AGNs were found based on the *ISO* data (Genzel et al. 1998; Rigopoulou et al. 1999), which may be the result of the determination of the continuum level.

Finally, for IRAS 05189−2524, the flux and equivalent width of the 3.3 μm PAH emission estimated by an *ISO* spectrum obtained using a larger ($24'' \times 24''$) aperture (Clavel et al. 2000) are a factor of ~ 6 larger than the estimate in this paper. If the larger values are correct, the bulk of the 3.3 μm PAH emission detected in the *ISO* spectrum must originate in extended star-forming regions outside the CGS4 slit. The extended star formation regions could explain nearly all of the far-infrared luminosity of this source, if the value of $L_{3.3}/L_{\rm FIR} = 1.7\text{–}1.9 \times 10^{-3}$ is adopted. However, this source shows no extended continuum emission at 12–25 μm (Soifer et al. 2000). If the extended regions are fully responsible for the far-infrared emission at 60 μm but contribute to, say, less than 5% of the 25 μm flux (Soifer et al. 2000), then the 60 μm to 25 μm flux ratio in Jy is greater than 80, much larger than any nearby star-forming galaxies (Rice et al. 1988). Since the physical conditions in the extended regions of IRAS 05189−2524 (not nuclear compact regions that could have an extreme environment in density and so on) are expected not to be quite different from those in nearby star-forming galaxies, such a sudden flux increase from the mid-infrared (<25 μm) to far-infrared (>40 μm) only in the case of IRAS 05189−2524 is very unlikely. While the 3.3 μm PAH flux in this paper is estimated by tracing the spectral profile (see the caption of Table 4 for more details), Clavel et al. (2000) simply sum up all the flux above the adopted continuum level in the predefined wavelength range (J. Clavel 2000, private communication). The *ISO* spectrum provided by J. Clavel (2000, private communication) shows a flux excess above an adopted continuum level at ~ 3.3 μm, but it has lower spectral resolution ($R \sim 100$) and larger scatter in data points at 3–4 μm than the CGS4 spectrum. Furthermore, although the wavelength of the 3.3 μm PAH emission feature usually extends from 3.24 to 3.34 μm in the rest-frame (Tokunaga et al. 1991; this paper), the flux excess in the *ISO* spectrum is found from 3.25 to 3.40 μm (not 3.34 μm). If this excess is actually due to the 3.3 μm PAH emission feature, its spectral shape in the extended regions of IRAS 05189−2524 is quite different from typical ones. More sensitive and higher spectral resolution spectroscopy with a wide aperture is necessary to address this issue. We tentatively consider that the extended regions contribute little to the total far-infrared luminosity of IRAS 05189−2524.

5.4.2. *8–25 μm Imaging Studies*

Soifer et al. (2000) suggested based on their 8–25 μm imaging data that AGN activity is the dominant energy source of Mrk 231, IRAS 05189−2524, and IRAS 08572+3915. Our conclusions are the same for these three sources. Soifer et al. (2000) were unable to distinguish the energy source of Mrk 273 and Arp 220. We argue that AGN activity is the main energy source of Mrk 273, while the energy source of Arp 220 is not clear. As a whole, the conclusions in this paper are consistent with those by Soifer et al. (2000).

5.4.3. *2 μm Spectroscopy*

In the less than 2 μm spectra of Mrk 231, IRAS 05189−2524, IRAS 23060+0505, and IRAS 20460+1925, a broad (>2000 km s^{-1} in FWHM) component of neutral hydrogen recombination line emission was detected, and their intrinsic luminosities are high enough to account for the far-infrared luminosities resulting from AGN activity alone (Veilleux, Sanders, & Kim 1999b). Our suggested energy source for these four IRLGs are consistent with theirs.

5.4.4. *Summary of the Above Comparison*

Among the nine IRLGs, five (Mrk 231, IRAS 05189−2524, IRAS 08572+3915, IRAS 23060+0505, and IRAS 20460+1925) have warm (*IRAS* 25 μm to 60 μm flux ratio $f_{25}/f_{60} > 0.2$) far-infrared color (Table 1). The above three infrared diagnoses have provided a growing amount of evidence that these warm IRLGs are powered predominantly by AGN activity (Table 5). However, warm IRLGs constitute only $\sim 20\%$ of total IRLGs, and most IRLGs have cool ($f_{25}/f_{60} < 0.2$) far-infrared color (Kim & Sanders 1998). It was argued based on the estimate of the 7.7 μm PAH strengths in the *ISO* spectra that these cool IRLGs are powered predominantly by starburst activity, with little AGN contribution (Genzel & Cesarsky 2000). Among the nine IRLGs, three (Arp 220, NGC 6240, and Mrk 273) are cool IRLGs and are classified as starburst-dominated IRLGs based on the 7.7 μm PAH strength (Table 5). However, for Arp 220 and Mrk 273, our 3–4 μm spectra suggest that the 7.7 μm PAH strengths, and thereby the magnitudes of starburst activity, may be overestimated based on the *ISO* spectra. In fact, for Mrk 273, although the relative 7.7 μm PAH emission strength suggests that this source is powered by starburst activity (Rigopoulou et al. 1999), a different diagnosis based on high excitation lines in the *ISO* spectra indicates that AGN activity is a dominant energy source (Genzel et al. 1998). For NGC 6240, X-ray data suggest that highly embedded and highly luminous AGN activity is an important energy source (Vignati et al. 1999). The contribution of AGN activity in the cool IRLGs may be higher than the estimate based on the 7.7 μm PAH emission strength in the *ISO* spectra.

5.4.5. *Compact Radio Core Emission*

High spatial resolution radio images have been used to investigate the relative importance between AGN and starburst activity in IRLGs. A compact radio core, which was thought to be strong evidence for AGN activity, is no longer definitive evidence for AGN activity because both AGN and compact starburst activity could explain observed properties of the compact radio core (Smith, Lonsdale, & Lonsdale 1998). However, IRLGs whose radio emission morphology is extended without a compact core are thought to be powered by starburst activity. Compact radio cores were detected in IC 694, Arp 220, NGC 6240, Mrk 273, Mrk 231, and IRAS 20460+1925 (Lonsdale, Lonsdale, & Smith 1992; Lonsdale, Smith, & Lonsdale 1993; Heisler et al. 1998; Kewley et al. 2000), but not in IRAS 05189+2524, IRAS 08572+3915, and IRAS 23060+0505 (Lonsdale et al. 1993; Heisler et al. 1998). It is puzzling that no radio core emission was detected in the

three warm IRLGs, for which more than one infrared diagnosis consistently suggests that AGN activity is a dominant energy source (Table 5).

5.5. *Future Study*

A high fraction ($\frac{6}{9}$) of IRLGs in this sample are suggested to be powered by AGN activity. This is probably caused by the selection effect of picking IRLGs that are bright at 3–4 μm. At a given far-infrared flux, the 3–4 μm flux of less obscured AGNs is generally higher than that of starburst-dominated galaxies (Schmitt et al. 1997). Among the nine IRLGs, $\frac{5}{9}$ (55%) are optically classified as Seyfert types (Table 1) and $\frac{4}{9}$ (44%; Mrk 231, IRAS 05189−2524, IRAS 23060+1925, and IRAS 23060+0505) show a detectable broad emission line at less than 2 μm (that is, AGN activity is less obscured). These fractions are significantly higher than those in a larger sample of IRLGs (∼20%; Veilleux, Kim, & Sanders 1999a; Veilleux et al. 1999b). Furthermore, the fraction of warm IRLGs in this sample ($\frac{5}{9}$; 55%) is much higher than that in a larger sample of IRLGs (∼20%; Kim & Sanders 1998). Observations of a larger number of fainter IRLGs at L are clearly necessary to evaluate the relative role between AGN and starburst activity in IRLGs as a whole.

6. SUMMARY

The energy sources of nine IRLGs were diagnosed using the $EW_{3.3}$ values and the $L_{3.3}/L_{FIR}$ ratios. The following main results were found:

1. Mrk 231, Mrk 273, and IRAS 05189−2524 show detectable 3.3 μm PAH emission in their 3–4 μm spectra. However, the PAH emission strengths are too small to account for the bulk of their far-infrared luminosities by starburst activity, indicating that these sources are powered by AGN activity.

2. No PAH emission was detected in the spectra of IRAS 08572+3915, IRAS 23060+0505, and IRAS 20460+1925. It was suggested that IRAS 08572+3915 is powered by highly obscured AGN activity, while IRAS 23060+0505 and IRAS 20460+1925 are powered by less obscured AGN activity.

3. For IC 694, Arp 220, and NGC 6240, while the $EW_{3.3}$ values are as large as those of starburst galaxies, the $L_{3.3}/L_{FIR}$ ratios after correction for screen dust extinction are a factor of ∼3 smaller. Whether these three IRLGs are powered by starburst activity only or obscured AGN activity contributes significantly is not clear because the actual dust extinction correction factor could be higher than our estimate and the scatter of the intrinsic $L_{3.3}/L_{FIR}$ ratios for starburst activity is poorly known.

4. Our energy diagnoses reinforced the previous suggestions that AGN activity is the dominant energy source in warm IRLGs.

We thank T. Kerr, J. Davies, T. Carroll, and T. Wold for their support during the UKIRT observing runs. We are grateful to D. B. Sanders and the anonymous referee for their useful comments. A. T. Tokunaga and H. Ando gave M. I. the opportunity to work at the University of Hawaii. L. Good kindly proofread this paper, and K. Teramura modified Figure 1. The United Kingdom Infrared Telescope is operated by the Joint Astronomy Centre on behalf of the U.K. Particle Physics and Astronomy Research Council. M. I. is financially supported by the Japan Society for the Promotion of Science during his stay at the University of Hawaii. C. C. D. gratefully acknowledges the National Research Council (USA), the Naval Research Laboratory, and the Office of Naval Research for their generous support and the sponsorship of J. Fischer.

APPENDIX

COMPARISONS WITH PREVIOUS 3–4 μm SPECTRA

Our new spectra (mostly higher signal-to-noise ratios and spectral resolution) are compared with old spectra in the literature.

IC 694.—A flux-calibrated 3–4 μm spectrum taken with a 2.″7 aperture was presented by Dennefeld & Desert (1990). The overall spectral shape and flux level in the new spectrum are consistent with the previous spectrum. Using narrowband filters, Satyapal et al. (1999) estimated the flux of the 3.3 μm PAH emission to be 8.5×10^{-13} ergs s^{-1} cm^{-2} within a 7″ aperture. This is ∼40% higher than our estimate, but this difference does not affect our discussion significantly.

Arp 220 and NGC 6240.—Low-resolution spectra taken using a circularly variable filter with an 8.″7 aperture were presented by Rieke et al. (1985). They showed strong 3.3 μm PAH emission. The new spectra show slightly smaller continuum flux levels but similar spectral shapes.

Mrk 231.—A flux-calibrated 3–4 μm spectrum taken with a 3.″8 aperture was presented by Imanishi et al. (1998). The new spectrum provides much higher signal-to-noise ratios. The spectral shape and flux level are consistent with the previous spectrum.

IRAS 05189−2524.—A flux-uncalibrated 3–4 μm spectrum was presented by Wright et al. (1996). It showed weak 3.3 μm PAH emission and weak 3.4 μm carbonaceous dust absorption with an optical depth of ∼0.05. The new spectrum is consistent with the previous spectrum in the spectral shape and the optical depth of the carbonaceous dust absorption.

IRAS 08572+3915.—A flux-uncalibrated 3–4 μm spectrum was presented by Wright et al. (1996). It was dominated by the 3.4 μm carbonaceous dust absorption feature, and its optical depth was estimated to be ∼0.9 (Pendleton 1996). Both the spectral shape and the optical depth in the new spectrum are consistent with the previous spectrum.

IRAS 23060+0505.—Wright et al. (1996) classified the 3–4 μm spectrum of IRAS 23060+0505 as featureless. The new spectrum is consistent with their classification.

NGC 253.—A low-resolution spectrum taken using a circularly variable filter with a 7.″5 aperture was presented by Moorwood (1986). Both the new and old spectra show the PAH emission at 3.3 and 3.4 μm. The flux level in our new spectrum is smaller than the old spectrum because of smaller aperture size.

REFERENCES

Alonso-Herrero, A., Rieke, G. H., Rieke, M. J., & Scoville, N. Z. 2000, ApJ, 532, 845
Armus, L., Heckman, T. M., & Miley, G. K. 1989, ApJ, 347, 727
Blain, A. W., Kneib, J.-P., Ivison, R. J., & Smail, I. 1999, ApJ, 512, L87
Brand, P. W. J. L., Moorhouse, A., Burton, M. G., Geballe, T. R., Bird, M., & Wade, R. 1988, ApJ, 334, L103
Bridger, A., Wright, C. S., & Geballe, T. R. 1994, in Infrared Astronomy with Arrays: The Next Generation, ed. I. McLean (Dordrecht: Kluwer), 537
Clavel, J., et al. 2000, A&A, 357, 839
Dennefeld, M., & Desert, F. X. 1990, A&A, 227, 379
Dudley, C. C. 1999, MNRAS, 307, 553
Dudley, C. C., & Wynn-Williams, C. G. 1997, ApJ, 488, 720
Elbaz, D., et al. 1998, in Proc. 34th Liege Internat. Astrophys. Colloq., The Next Generation Space Telescope: Science Drivers and Technological Challenges, 47 (astro-ph/9807209)
Engelbracht, C. W., Rieke, M. J., Rieke, G. H., Kelly, D. M., & Achtermann, J. M. 1998, ApJ, 505, 639
Frogel, J. A., Gillett, F. C., Terndrup, D. M., & Vader, J. P. 1989, ApJ, 343, 672
Genzel, R., & Cesarsky, C. J. 2000, ARA&A, in press (astro-ph/0002184)
Genzel, R., et al. 1998, ApJ, 498, 579
Genzel, R., Weitzel, L., Tacconi-Garman, L. E., Blietz, M., Cameron, M., Krabbe, A., & Lutz, D. 1995, ApJ, 444, 129
Glass, I. S., & Moorwood, A. F. M. 1985, MNRAS, 214, 429
Goldader, J. D., Joseph, R. D., Doyon, R., & Sanders, D. B. 1995, ApJ, 444, 97
Heisler, C. A., Norris, R. P., Jauncey, D. L., Reynolds, J. E., & King, E. A. 1998, MNRAS, 300, 1111
Hill, G. J., Wynn-Williams, C. G., & Becklin, E. E. 1987, ApJ, 316, L11
Imanishi, M., Terada, H., Goto, M., & Maihara, T. 1998, PASJ, 50, 399
Imanishi, M., Terada, H., Sugiyama, K., Motohara, K., Goto, M., & Maihara, T. 1997, PASJ, 49, 69
Imanishi, M., & Ueno, S. 2000, ApJ, 535, 626
Ivezic, Z., Nenkova, M., & Elitzur, M. 1999, Users Manual for DUSTY, Univ. Kentucky Internal Rep. (astro-ph/9910475)
Joy, M., Telesco, C. M., Decher, R., Lester, D. F., Harvey, P. M., Rickard, L. J., & Bushouse, H. 1989, ApJ, 339, 100
Kalas, P., & Wynn-Williams, C. G. 1994, ApJ, 434, 546
Kewley, L. J., Heisler, C. A., Dopita, M. A., Sutherland, R., Norris, R. P., Reynolds, J., & Lumsden, S. 2000, ApJ, 530, 704
Kim, D.-C., & Sanders, D. B. 1998, ApJS, 119, 41
Laureijs, R. J., et al. 2000, A&A, 359, 900
Lonsdale, C. J., Lonsdale, C. J., & Smith, H. E. 1992, ApJ, 391, 629
Lonsdale, C. J., Smith, H. E., & Lonsdale, C. J. 1993, ApJ, 405, L9
Lutz, D., et al. 1996, A&A, 315, L269
Lutz, D., Spoon, H. W. W., Rigopoulou, D., Moorwood, A. F. M., & Genzel, R. 1998, ApJ, 505, L103
Maloney, P. R. 1999, Ap&SS, 266, 207
Mathis, J. S. 1990, ARA&A, 28, 37
Moorwood, A. F. M. 1986, A&A, 166, 4
Mountain, C. M., Robertson, D. J., Lee, T. J., & Wade, R. 1990, Proc. SPIE, 1235, 25
Mouri, H., Kawara, K., Taniguchi, Y., & Nishida, M. 1990, ApJ, 356, L39
Pendleton, Y. 1996, in The Cosmic Dust Connection, ed. J. M. Greenberg (Dordrecht: Kluwer), 71
Pendleton, Y. J., Sandford, S. A., Allamandola, L. J., Tielens, A. G. G. M., & Sellgren, K. 1994, ApJ, 437, 683
Rice, W., Lonsdale, C. J., Soifer, B. T., Neugebauer, G., Kopan, E. L., Lloyd, L. A., De Jong, T., & Habing, H. J. 1988, ApJS, 68, 91
Rieke, G. H., Curti, R. M., Black, J. H., Kailey, W. F., McAlary, C. W., Lebofsky, M. J., & Elston, R. 1985, ApJ, 290, 116
Rieke, G. H., & Lebofsky, M. J. 1985, ApJ, 288, 618
Rieke, G. H., Lebofsky, M. J., Thompson, R. I., Low, F. J., & Tokunaga, A. T. 1980, ApJ, 238, 24
Rigopoulou, D., Spoon, H. W. W., Genzel, R., Lutz, D., Moorwood, A. F. M., & Tran, Q. D. 1999, AJ, 118, 2625
Roche, P. F., Aitken, D. K., Smith, C. H., & Ward, M. J. 1991, MNRAS, 248, 606
Rudy, R. J., Levan, P. D., & Rodriguez-Espinosa, J. M. 1982, AJ, 87, 598
Sanders, D. B., & Mirabel, I. F. 1996, ARA&A, 34, 749
Satyapal, S., Watson, D. M., Forrest, W. J., Pipher, J. L., Fischer, J., Greenhouse, M. A., Smith, H. A., & Woodward, C. E. 1999, ApJ, 516, 704
Schmitt, H. R., Kinney, A. L., Calzetti, D., & Bergmann, T. S. 1997, AJ, 114, 592
Scoville, N. Z., et al. 2000, AJ, 119, 991
Smith, H. E., Lonsdale, C. J., & Lonsdale, C. J. 1998, ApJ, 492, 137
Soifer, B. T., et al. 2000, AJ, 119, 509
Soifer, B. T., Sanders, D. B., Madore, B. F., Neugebauer, G., Danielson, G. E., Elias, J. H., Lonsdale, C. J., & Rice, W. L. 1987, ApJ, 320, 238
Sugai, H., Davies, R. I., Malkan, M. A., McLean, I. S., Usuda, T., & Ward, M. J. 1999, ApJ, 527, 778
Sugai, H., Malkan, M. A., Ward, M. J., Davies, R. I., & McLean, I. S. 1997, ApJ, 481, 186
Surace, J. A., & Sanders, D. B. 1999, ApJ, 512, 162
Surace, J. A., Sanders, D. B., & Evans, A. S. 2000, ApJ, 529, 170
Tokunaga, A. T. 2000, in Allen's Astrophysical Quantities, ed. A. N. Cox (4th ed; New York: AIP), chap. 7, 143
Tokunaga, A. T., Sellgren, K., Smith, R. G., Nagata, T., Sakata, A., & Nakada, Y. 1991, ApJ, 380, 452
Tully, R. B. 1988, in Nearby Galaxies Catalog (Cambridge: Cambridge Univ. Press), 10
Vader, J. P., Frogel, J. A., Terndrup, D. M., & Heisler, C. A. 1993, AJ, 106, 1743
Veilleux, S., Kim, D.-C., & Sanders, D. B. 1999a, ApJ, 522, 113
Veilleux, S., Kim, D.-C., Sanders, D. B., Mazzarella, J. M., & Soifer, B. T. 1995, ApJS, 98, 171
Veilleux, S., Sanders, D. B., & Kim, D.-C. 1999b, ApJ, 522, 139
Vignati, P., et al. 1999, A&A, 349, L57
Voit, G. M. 1992, MNRAS, 258, 841
Wright, G. S., Bridger, A., Geballe, T. R., & Pendleton, Y. 1996, in New Extragalactic Perspectives in the New South Africa, ed. D. L. Block & J. M. Greenberg (Dordrecht: Kluwer), 143
Zhou, S., Wynn-Williams, C. G., & Sanders, D. B. 1993, ApJ, 409, 149